

The Role of Carrier Injection in the Breakdown Mechanism of Amorphous Al_2O_3 Layers

P. La Torraca, A. Padovani, *Member, IEEE*, J. Strand, A. Shluger, L. Larcher

Abstract—We investigated the dielectric breakdown (BD) mechanism in amorphous alumina ($\text{a-Al}_2\text{O}_3$) metal-insulator-metal (MIM) stacks. Density functional theory (DFT) calculations reveal oxygen vacancy (V_O) generation in $\text{a-Al}_2\text{O}_3$ occurs via thermochemical (TC) bond-breaking and, more efficiently, via newly discovered pathways enabled by charge trapping in under-coordinated Al ions (UC_Al) and in existing V_O s. Multiscale simulations show the importance of these processes, which allow explaining the experimental BD dynamics in $\text{a-Al}_2\text{O}_3$, and provide valuable insights into the role of carriers' injection in the degradation and reliability of high-k materials.

Index Terms— Amorphous alumina, atomic defects, breakdown, carrier injection, high-k dielectric

I. INTRODUCTION

DESPITE the widespread applications of $\text{a-Al}_2\text{O}_3$ as a high-k gate oxide [1-3], and in signal [4] and memory capacitors [5,6], its degradation mechanism is still unclear. The current understanding is based on the TC model of bond-breaking [7,8], according to which current-carrying defects, such as V_O s, are generated by the rupture of the Al-O bonds as a result of an electric field application and the dielectric's polarization. A bond-breaking activation energy (E_A) around 2.4 eV was extracted from experimental results on $\text{a-Al}_2\text{O}_3$ [8]. In contrast, for a stable pair of V_O and O interstitial (O_i) in crystalline $\alpha\text{-Al}_2\text{O}_3$, formation energies between 5.8 and 11.8 eV have been calculated [9-11], with the corresponding bond-breaking E_AS even higher. Although different E_AS are expected for the different Al_2O_3 phases, the huge discrepancy (>3 eV) suggests the involvement of other processes in the BD. For example, according to the carrier injection (CI) breakdown model [12], the injection and localization of carriers in perfect or defective lattice can weaken the adjacent metal-oxygen bonds, promoting the field-induced bond-breaking processes and enabling V_O s generation pathways. The effectiveness of the CI mechanism has been shown in SiO_2 [12] and HfO_2 [13].

In this work, we show that the CI mechanism can correctly describe the dielectric BD in $\text{a-Al}_2\text{O}_3$ MIM stacks, while reconciling the theoretical and experimental E_AS . DFT calculations are used to characterize the $\text{a-Al}_2\text{O}_3$ defects and

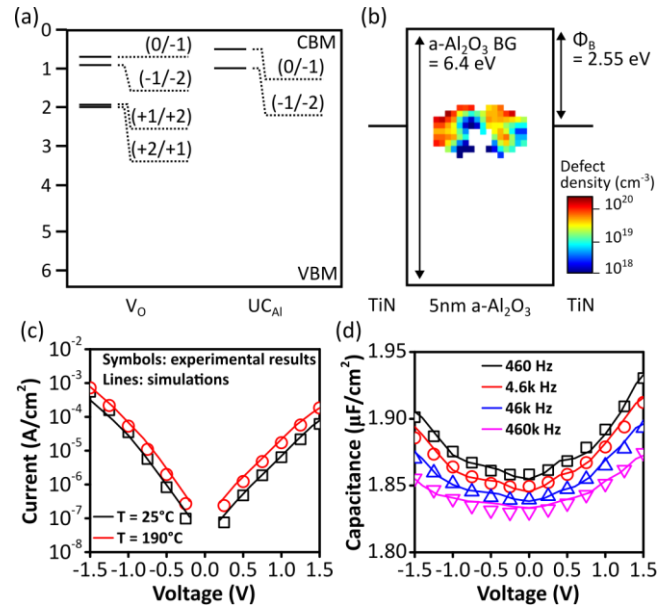


Figure 1. (a) The calculated charge transition levels (corresponding to thermal ionization energies E_THS) for V_O s and UC_Al s in $\text{a-Al}_2\text{O}_3$; (b) extracted space-energy defect distribution in a 5 nm $\text{TaN}/\text{a-Al}_2\text{O}_3/\text{TaN}$ MIM stack, compatible with $+2/+1$ and $+1/0$ transition of V_O s; (c) current and (d) capacitance simulation of the 5 nm $\text{TaN}/\text{a-Al}_2\text{O}_3/\text{TaN}$ MIM stack.

their generation processes, showing how the electron injection into structural precursor sites, formed by UC_Al s or existing V_O s, greatly facilitate the creation of new V_O s. Using the commercial simulation software Ginestra® [14], we show that the resulting electrical characteristics and BD statistics agree with the experimental results, demonstrating the paramount importance of electron injection for the $\text{a-Al}_2\text{O}_3$ -based devices' reliability.

II. DENSITY FUNCTIONAL THEORY CALCULATIONS

DFT calculations are carried out using the CP2K [15] software package. Exchange-correlation (XC) energy is calculated using the PBE0-TC-LRC functional [16], providing a more accurate description of the electronic structure and the localized states of oxides when compared to standard Generalized Gradient Approximation (GGA) functionals. The $\text{a-Al}_2\text{O}_3$ structures are produced as described in [17] with resulting band gaps (BGs) in the 6 to 7 eV range. The analysis of the electronic properties of $\text{a-Al}_2\text{O}_3$ models showed that V_O s and pairs of 4-coordinated Al ions (i.e. UC_Al s) can trap electrons

P. L.T. is with the Department of Science and Methods for Engineering, University of Modena and Reggio Emilia, Reggio Emilia, Italy and with the Tyndall National Institute, University College Cork, Cork, Ireland. (e-mail: paolo.latorraca@tyndall.ie)

A. P. is with the Engineering Department "Enzo Ferrari", University of Modena and Reggio Emilia, Reggio Emilia, Italy.

J. S. and A. S. are with the Department of Physics and Astronomy, University College London, London, United Kingdom.

L. L. is with Applied Materials – MDLx Italy R&D, Reggio Emilia, Italy.

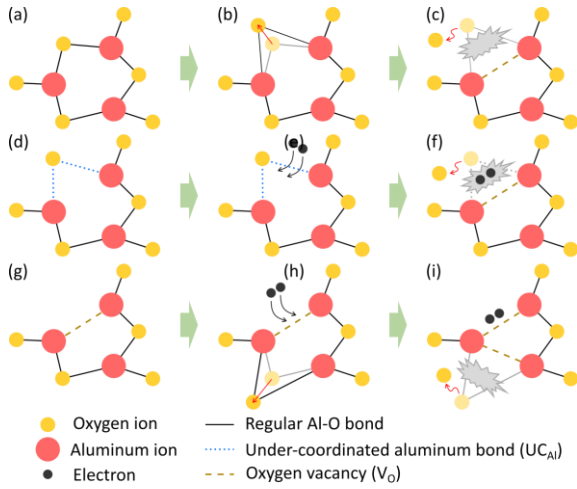


Figure 2. Schematic representation of different V_O generation pathways: a typical O-Al-O bond (a) stretched by an electric field (b) breaks generating a V_O (c); a structural precursor site (d) traps two electrons (e) facilitating the creation of $V_O - O_I^{-2}$ pair (f); a V_O (g) traps two electrons (h), facilitating the creation of the second V_O and O_I^{-2} ion (i). The TC model only accounts for the former process (a-c), while the CI model includes all three depicted processes.

in states within the a- Al_2O_3 BG, depicted in Fig. 1(a). The respective thermal ionization energies (E_{THS}) and relaxation energies (E_{RELS}) are reported in Table I.

The bond-breaking process is simulated in different a- Al_2O_3 structures using the nudged elastic band (NEB) method [18], including the electric field effects [19]. The most relevant V_O generation processes identified from the simulations are depicted in Fig. 2 and the respective E_{AS} are summarized in Table I. In the simulated systems, the TC bond-breaking process creates $V_O^{+2} - O_I^{-2}$ pairs, Fig. 2(a-c). While not requiring electron localization, this process is characterized by a relatively high bond-breaking E_{AS} range. The negative charging of UC_{AIS} and V_O s from CI into their shallow states enables more efficient V_O s generation pathways. The double electron trapping in a UC_{AIS} , Fig. 2(d-f), lowers the bond-breaking E_A facilitating the generation of V_O s through the conversion of UC_{AIS} 's into $V_O^0 - O_I^{-2}$ pairs. Pre-existing V_O s, either present in the pristine system or generated by the electrical stress, are also identified as precursor sites for new V_O s. The quadruple electron trapping in a pre-existing V_O induces a distortion in the adjacent bonds, lowering their bond-breaking E_A and thus facilitating the generation of a new V_O , Fig 2(g-i). While only a small share of V_O s ($\sim 1\%$) are stable in the negative charge states, required for enabling the described process, all poly-vacancy clusters are capable of negative charging, facilitating the V_O s generation as in Fig. 2(g-i).

TABLE I

A- Al_2O_3 DEFECTS' AND DEGRADATION PROCESSES' PARAMETERS		
Parameter	DFT calculation	Simulation
Under-coordinated Al ion		
-2/-1 E_{TH} / E_{REL}	1.0 eV / 1.0 eV	1.4 ± 0.5 eV / 1.0 eV
-1/0 E_{TH} / E_{REL}	0.5 eV / 0.5 eV	0.9 ± 0.5 eV / 1.0 eV
Oxygen vacancy		
-2/-1 E_{TH} / E_{REL}	0.9 eV / 1.5 eV	1.3 ± 0.5 eV / 1.5 eV
-1/0 E_{TH} / E_{REL}	0.7 eV / 1.3 eV	1.1 ± 0.5 eV / 1.3 eV
0/+1 E_{TH} / E_{REL}	1.9 eV / 1.6 eV	2.3 ± 1 eV / 1.6 eV
+1/+2 E_{TH} / E_{REL}	2.0 eV / 1.0 eV	2.4 ± 1 eV / 1.0 eV
TC bond breaking E_A	3 – 6 eV	4.3 eV
$UC_{AIS}^{-2} \rightarrow V_O^0 - O_I^{-2}$ E_A	2.0 – 3.0 eV	2.5 eV
$V_O^{-2} \rightarrow 2V_O^0 - 2O_I^{-2}$ E_A	3.0 eV	2.8 eV

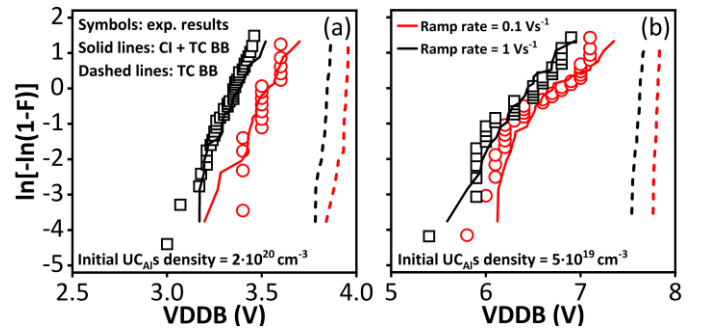


Figure 3. Experimental (symbols) and simulated (lines) VDDB distributions of (a) 5 nm and (b) 10 nm TaN/a- Al_2O_3 /TaN stacks [8], under RSV with 0.1 Vs^{-1} (red) and 1 Vs^{-1} (black) ramp rate. Simulations are obtained with the bond-breaking E_A s presented in this work (Table I). The TC bond-breaking process (TC model, in dashed lines) alone overestimates the VDDB. Including the bond-breaking processes enabled by charge trapping at the defects (CI + TC model, in solid lines), shown in Fig. 2, allow reproducing the VDDB statistics. The statistical spread is reproduced considering different UC_{AIS} initial densities.

III. MULTISCALE SIMULATIONS

The results of DFT calculations were used to investigate the a- Al_2O_3 BD dynamics of TaN/a- Al_2O_3 /TaN MIM with Ginestra® [14]. This approach allows us to self-consistently include the devices' electrostatics, carriers' trapping and transport (according to the multiphonon trap-assisted tunneling model [20]), and all the degradation processes illustrated in Fig. 2.

Fig. 1(b) shows the space-energy defect distribution of a 5 nm TaN/a- Al_2O_3 /TaN MIM stack, extracted via defect spectroscopy from the current-voltage (IV) curves, Fig. 1(c), and capacitance-voltage (CV) curves, Fig. 1(d), reported in [8]. The extracted defects' E_{TH} is distributed from 1.9 eV to 3.2 eV and peaks near 2.0 eV, which is consistent with the DFT results for the (+2/+1) and the (+1/0) transition levels of V_O s. As in SiO_2 [21,22] and HfO_2 [20,22], V_O s are thus recognized as the main defects involved in electron transport and trapping in a- Al_2O_3 . The shallower transition levels of V_O s and UC_{AIS} do not contribute to the transport nor to the AC response in the voltage range considered in Fig. 1. This highlights the elusive nature of the UC_{AIS} , that cannot be effectively detected and characterized with regular electrical characterization techniques (e.g. IV or CV measurements). Nevertheless, their effects could be observed in the oxide degradation dynamics: the application of a sufficiently high field allows charge trapping and transport even in such shallow levels, possibly triggering the CI-related degradation processes described in the Section II and Fig. 2.

The breakdown dynamics and the critical role played by the V_O s and the UC_{AIS} is investigated simulating the voltage dependent dielectric breakdown (VDDB) statistics of 5 nm and 10 nm TaN/a- Al_2O_3 /TaN MIM stacks under ramped voltage stress (RVS) at different ramp rates (0.1 and 1 Vs^{-1}), also reported in [8]. Fig. 3 shows the simulation results obtained using the parameters listed in Table I, considering the TC bond breaking process alone (dashed lines) and by including the CI-related degradation processes (solid lines), i.e. all processes depicted in Fig. 2. The sole TC bond breaking process greatly overestimates the BD voltages and cannot explain the lower

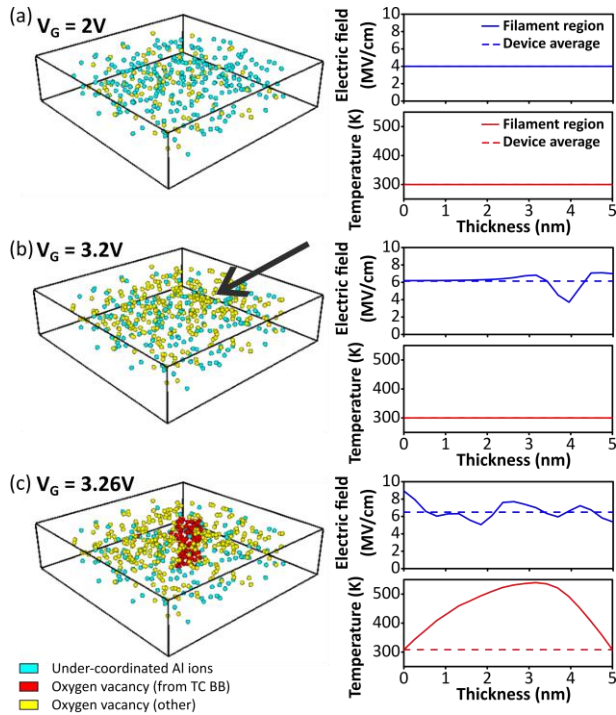


Figure 4. Breakdown dynamics in a 5nm TaN/a-Al₂O₃/TaN MIM. Starting from a pristine device with V_{OS} and UC_{AlS} distributions, the defect generation starts at approximately 4 MVcm^{-1} (a) via CI-related processes alone. Upon the formation of a large V_{OS} cluster (b) the oxide local permittivity is reduced, enhancing the surrounding electric field and initiating the TC bond breaking. A conductive filament is rapidly formed (c), driving an increasingly higher current. The resulting increment of the local temperature facilitates the TC V_{OS} generation, initiating a thermal runaway that ends in the device hard breakdown.

Weibull slope in the 10 nm stack. Including the CI-related degradation processes, the whole VDDB statistics is correctly reproduced. The pathways enabled by the CI allow for a more efficient V_{OS} generation, facilitating the BD process and thus reducing the BD voltage. The lower slope exhibited by the 10 nm stack results from a lower UC_{AlS} density in the pristine device: in a less defective device, a larger number of defects must be generated for the formation of a BD spot, increasing the statistical variability of the degradation process, which translates in a lower Weibull slope [22]. This result agrees with the previous results on a-Al₂O₃ defectivity, based on IV curve fitting [8], showing a higher defectivity in a 5 nm layer than in 10 nm and 20 nm layers, possibly due to the different growth time and thermal budget.

Fig. 4 shows the degradation process in the simulated 5 nm a-Al₂O₃ stack. In a pristine device, Fig. 4(a), both V_{OS} and UC_{AlS} are present, with the former contributing to the leakage current shown in Fig. 1(c). At approximately 4 MVcm^{-1} (2 V), the CI into the UC_{AlS} enables the generation of new V_{OS} , which in turn can also generate new V_{OS} , following the pathways shown in Fig. 2. The relatively low E_{AS} of these mechanisms provide an efficient and self-sustaining generation of V_{OS} , without the TC bond-breaking contribution. This generation process leads to the formation of V_{OS} clusters, close to the location of the starting UC_{AlS} . When a sufficiently large cluster of V_{OS} is formed, Fig. 4(b), the permittivity reduction associated to the metallic nature of that cluster leads to the

redistribution of the internal electric field. A significant enhancement of the electric field above and below the V_{OS} cluster is sufficient to trigger the TC bond breaking in these regions, longitudinally extending the cluster into a full BD spot, Fig. 4(c). The current flowing in the forming BD spot increases the local temperature, further facilitating the V_{OS} generation, leading to a thermal runaway and the device hard BD.

IV. CONCLUSIONS

We presented a comprehensive study, including DFT calculations and multiscale simulations, fully explaining the breakdown dynamics in a-Al₂O₃ MIM stacks within the CI model framework. The discrepancy between the theoretical TC bond-breaking E_A values and the experimental results is explained by the interplay of other V_{OS} generation pathways, enabled by charge trapping in pre-existing UC_{AlS} and V_{OS} .

REFERENCES

- [1] T. L. Newsom, C. R. Allemang, T. H. Cho, N. P. Dasgupta and R. L. Peterson, "59.9 mV·dec Subthreshold Swing Achieved in Zinc Tin Oxide

- TFTs With In Situ Atomic Layer Deposited AlO Gate Insulator," in *IEEE Electron Device Letters*, vol. 44, no. 1, pp. 72-75, Jan. 2023, doi: 10.1109/LED.2022.3219351.
- [2] Y. -C. Chien *et al.*, "Origin of High Current and Illumination Stress Instability in Self-Aligned α -InGaZnO Thin Film Transistors With Al₂O₃ as High- κ Gate Dielectric," in *IEEE Electron Device Letters*, vol. 41, no. 4, pp. 565-568, April 2020, doi: 10.1109/LED.2020.2976616.
- [3] M. -J. Yu, R. -P. Lin, Y. -H. Chang and T. -H. Hou, "High-Voltage Amorphous InGaZnO TFT With Al₂O₃ High- κ Dielectric for Low-Temperature Monolithic 3-D Integration," in *IEEE Transactions on Electron Devices*, vol. 63, no. 10, pp. 3944-3949, Oct. 2016, doi: 10.1109/TED.2016.2598396.
- [4] S.Y. Ko, J.I. Oh, J.C. Choi, K.H. Lee, Y.H. Bae, Y.C. Jung, Y.H. Lee, MIM Capacitors Using ALD Al₂O₃ for RF IC and DRAM Applications, *MRS Proc.* 833 (2004) 2-6, doi: 10.1557/proc-833-g3.10.
- [5] S.Y. Lee, J. Chang, J. Choi, Y. Kim, H.J. Lim, H. Jeon, H. Seo, Investigation of ultrathin Pt/ZrO₂-Al₂O₃-ZrO₂/TiN DRAM capacitors Schottky barrier height by internal photoemission spectroscopy, *Curr. Appl. Phys.* 17 (2017) 267-271, doi: 10.1016/j.cap.2016.12.004.
- [6] J. Park, S. Heo, J. Chung, G.-S. Park, Electron Energy Loss Spectroscopy Characterization of TANOS (TaN/Al₂O₃/Si₃N₄/SiO₂/Si) Stacks, *Microsc. Microanal.* 19 (2013) 109-113, doi: 10.1017/S1431927613012440.
- [7] J. W. McPherson, Jinyoung Kim, A. Shanware, H. Mogul and J. Rodriguez, "Trends in the ultimate breakdown strength of high dielectric-constant materials," in *IEEE Transactions on Electron Devices*, vol. 50, no. 8, pp. 1771-1778, Aug. 2003, doi: 10.1109/TED.2003.815141.
- [8] P. La Torraca, F. Caruso, A. Padovani, G. Tallarida, S. Spiga and L. Larcher, "Atomic Defects Profiling and Reliability of Amorphous Al₂O₃ Metal-Insulator-Metal Stacks," in *IEEE Transactions on Electron Devices*, vol. 69, no. 7, pp. 3884-3891, July 2022, doi: 10.1109/TED.2022.3172928.
- [9] X. Xiang, G. Zhang, X. Wang, T. Tang, and Y. Shi, "A new perspective on the process of intrinsic point defects in α -Al₂O₃," *Physical Chemistry Chemical Physics*, vol. 17, no. 43, Royal Society of Chemistry (RSC), pp. 29134-29141, 2015. doi: 10.1039/c5cp04867b.
- [10] A. Kononov, C.-W. Lee, E. P. Shapera, and A. Schleiße, "Identifying native point defect configurations in α -alumina," *Journal of Physics: Condensed Matter*, vol. 35, no. 33, IOP Publishing, p. 334002, May 18, 2023. doi: 10.1088/1361-648x/acd3cf.
- [11] Y. F. Zhukovskii, A. Platonenko, S. Piskunov, and E. A. Kotomin, "Ab initio simulations on migration paths of interstitial oxygen in corundum," *Nuclear Instruments and Methods in Physics Research Section B: Beam Interactions with Materials and Atoms*, vol. 374, Elsevier BV, pp. 29-34, May 2016. doi: 10.1016/j.nimb.2015.08.087.
- [12] A. Padovani, P. La Torraca, J. Strand, A. Shluger, V. Milo and L. Larcher, "Towards a Universal Model of Dielectric Breakdown," *2023 IEEE International Reliability Physics Symposium (IRPS)*, Monterey, CA, USA, 2023, pp. 1-8, doi: 10.1109/IRPS48203.2023.10117846.
- [13] J. Strand, P. La Torraca, A. Padovani, L. Larcher, and A. L. Shluger, "Dielectric breakdown in HfO₂ dielectrics: Using multiscale modeling to identify the critical physical processes involved in oxide degradation," *Journal of Applied Physics*, vol. 131, no. 23, AIP Publishing, p. 234501, Jun. 21, 2022. doi: 10.1063/5.0083189.
- [14] Applied Materials *GINESTRA*®
<https://www.appliedmaterials.com/eu/en/semiconductor/solutions-and-software/software-solutions/ginestra-simulation-platform.html>
- [15] J. VandeVondele, M. Krack, F. Mohamed, M. Parrinello, T. Chassaing, and J. Hutter, "Quickstep: Fast and accurate density functional calculations using a mixed Gaussian and plane waves approach," *Computer Physics Communications*, vol. 167, no. 2, Elsevier BV, pp. 103-128, Apr. 2005. doi: 10.1016/j.cpc.2004.12.014.
- [16] M. Guidon, J. Hutter, and J. VandeVondele, "Robust Periodic Hartree-Fock Exchange for Large-Scale Simulations Using Gaussian Basis Sets," *Journal of Chemical Theory and Computation*, vol. 5, no. 11, American Chemical Society (ACS), pp. 3010-3021, Oct. 20, 2009. doi: 10.1021/ct900494g.
- [17] O. A. Dicks and A. L. Shluger, "Theoretical modeling of charge trapping in crystalline and amorphous Al₂O₃," *Journal of Physics: Condensed Matter*, vol. 29, no. 31, IOP Publishing, p. 314005, Jul. 06, 2017. doi: 10.1088/1361-648x/aa7767.
- [18] H. Jónsson, G. Mills, and K. W. Jacobsen, "Nudged elastic band method for finding minimum energy paths of transitions," *Classical and Quantum Dynamics in Condensed Phase Simulations*. WORLD SCIENTIFIC, Jun. 1998. doi: 10.1142/9789812839664_0016.
- [19] J. W. Strand, J. Cottom, L. Larcher, and A. L. Shluger, "Effect of electric field on defect generation and migration in HfO₂," *Physical Review B*, vol. 102, no. 1, American Physical Society (APS), Jul. 21, 2020. doi: 10.1103/physrevb.102.014106.
- [20] L. Vandelli, A. Padovani, L. Larcher, R. G. Southwick, W. B. Knowlton and G. Bersuker, "A Physical Model of the Temperature Dependence of the Current Through SiO₂/HfO₂ Stacks," in *IEEE Transactions on Electron Devices*, vol. 58, no. 9, pp. 2878-2887, Sept. 2011, doi: 10.1109/TED.2011.2158825.
- [21] A. Padovani, D. Z. Gao, A. L. Shluger, and L. Larcher, "A microscopic mechanism of dielectric breakdown in SiO₂ films: An insight from multi-scale modeling," *Journal of Applied Physics*, vol. 121, no. 15, AIP Publishing, p. 155101, Apr. 21, 2017. doi: 10.1063/1.4979915.
- [22] A. Padovani and L. Larcher, "Time-dependent dielectric breakdown statistics in SiO₂ and HfO₂ dielectrics: Insights from a multi-scale modeling approach," *2018 IEEE International Reliability Physics Symposium (IRPS)*, Burlingame, CA, USA, 2018, pp. 3A.2-1-3A.2-7, doi: 10.1109/IRPS.2018.8353552.